Research article

Journal of RAMAN SPECTROSCOPY

Received: 19 October 2012 Revised: 1 January 2013 Accepted: 11 January 2013 Published online in Wiley Online Library: 2 March 2013

(wileyonlinelibrary.com) DOI 10.1002/jrs.4263

Structural transformations in a single-crystal Rb_2NaYF_6: Raman scattering study

A. S. Krylov,* A. N. Vtyurin, A. S. Oreshonkov, V. N. Voronov and S. N. Krylova

This paper reports Raman spectroscopy investigation of phase transitions in Rb_2NaYF_6 crystal. The experimental spectra were compared with the calculated one. The spectra were obtained in temperature range from 8 to 300 K. The Raman spectra shows anomalous temperature-dependent behavior at $T_1 = 154$ and $T_2 = 122$ K. Soft mode restoration has been found, which allows us to attribute first transition at 154 K to displacive type. Detailed analysis temperature dependencies of the line positions and widths have been performed. We found no effects of possible lattice disorder anywhere, except narrow (about 20 K) range above the T_1 temperature. The Raman spectra of Rb_2NaYF_6 crystal have been obtained and analyzed under hydrostatic pressure up to 4.33 GPa (at $T = 295$ K). The high pressure experiment up to 4.33 GPa did not disclose any effects associated with phase transitions. The lattice vibration spectra were calculated up to 10 GPa. The calculation has been demonstrated that the Rb_2NaYF_6 does not undergo high pressure phase transition. Copyright © 2013 John Wiley & Sons, Ltd.

Keywords: structural phase transition; Rb_2NaYF_6; hydrostatic pressure; calculation; lattice dynamics

Introduction

Rb_2NaYF_6 crystal doped with lanthanides attracts the special interest of investigators. Mroczkowski S. and Dorain P. demonstrated that single crystal Rb_2NaYF_6:Ce^{3+} can be successfully used for a broad-band laser tunable from 400 to 480 nm.[1] The emission and absorption properties of Rb_2NaYF_6 crystal doped with Yb^{3+} ions have been studied by Deloach *et al.*[2]; they considered it as a possible effective diode-pumped Yb^{3+} laser system. Bowman S. R. and Mungan C. E. presented Rb_2NaYF_6:Yb^{3+} as a new material for optical cooling.[3] Tanner and Faucher have investigated electronic absorption spectra of Rb_2NaYF_6:Tm^{3+} system.[4] Bucher E. *et al.* studied magnetic properties of Rb_2NaYF_6:Er^{3+} single crystal.[5] Aull B. F. and Jenssen H. P. studied Rb_2NaYF_6 single crystals, doped with Ce^{3+}, Er^{3+}, Nd^{3+}, or La^{3+}.[6] Ce-doped Rb_2NaYF_6 displays two distinct emitting centers, one in the blue and another in the near UV regions. So, six new materials based on Rb_2NaYF_6 crystal as a host lattice have been created by this time.

The perovskite-like Rb_2NaYF_6 crystal belongs to the family of elpasolites A_2BCX_6 with high symmetry phase G_0, space group $Fm\bar{3}m$, $Z = 4$, where A, B, and C are metal cations or more complex molecular ions, X is oxygen or halogen anions. This family of crystals has received special attention because of their simple cubic structure and isolated character of CX_6^{3-} complexes; they were considered as ideal host lattices for accommodating divalent and trivalent cations in perfect octahedral sites (C) of cubic crystal structure. It is a very perspective concept because host elpasolite family includes now more than 350 compounds, and crystal chemical analysis shows 1500 more that can be obtained only based on halides.[7] Synthesis, structures, spectra and energy transfer phenomena of lanthanide-containing elpasolites have been reviewed by Tanner.[8]

The structure of this Rb_2NaYF_6 host crystal at normal conditions was known from year 1968.[9,10] Its unit cell structure is shown in Fig. 1. The YF_6 octahedra are hatched units. The Y atom is assumed to be at the center of the octahedron, and an F atom at each vertex. In 40 years since the crystal discovery, there had been a number of studies of its structure and physical properties.[9–11] Yet, available sources provide no information on temperature and pressure transformations of this host structure, as well as on possible mechanisms of such transformations. Raman spectroscopy is a known informative method to study structural phase transitions in crystals.[12–15] The aim of this paper was to find the temperatures and pressure probable phase transitions and determine their mechanisms in this perspective host lattice material by Raman spectroscopy method.

Previous investigations of some elpasolites revealed soft mode condensations in low wavenumber region associated with the structural phase transitions.[16–18] Our working hypothesis was that Rb_2NaYF_6 crystal can undergo one or more temperature and pressure induced structural phase transitions, with soft modes condensation as well.

Experimental methods and data processing

The precursors taken in stoichiometric amounts were melted in platinum crucibles in argon atmosphere. After slow cooling, the boules with transparent inclusions were obtained. The single crystals were grown from selected transparent parts of the boules by Bridgeman–Stockbarger method at the hot zone temperature 1200 K (grad $T = 30$ K/cm, the pulling rate was 0.8 mm/hour) in the sealed platinum ampoules.[19] Samples for experiments ($1 \times 1 \times 1.5$ mm3) were optically transparent and without colored defects or inclusions visible under the microscope.

* Correspondence to: Alexander Krylov, L.V. Kirensky Institute of Physics SB RAS, 660036, Krasnoyarsk, Russia
E-mail: shusy@iph.krasn.ru

L. V. Kirensky Institute of Physics SB RAS, 660036, Krasnoyarsk, Russia

Raman spectra were collected using the polarized radiation of a 514.5 nm Ar^+ laser (Spectra-Physics Stabilite 2017) power 15 mW on the sample in the wavenumber region between 10 and 1200 cm^{-1}. The intensity of the laser light was adjusted to avoid sample heating. The spectra in the 180° geometry were recorded on a Horiba Jobin Yvon T64000 spectrometer equipped with a liquid Nitrogen cooled charge coupled device detection system in subtractive dispersion mode. The temperature studies were performed using an ARS CS204–X1.SS closed cycle helium cryostat. The temperature was measured by calibrated LakeShore DT–6SD1.4L silicon diode. The accuracy of temperature stabilization during spectra measurement was <0.2 K. The sample into an indium gasket was fixed on a coolant guide. Cryostat was evacuated to 1.0×10^{-6} mbar.

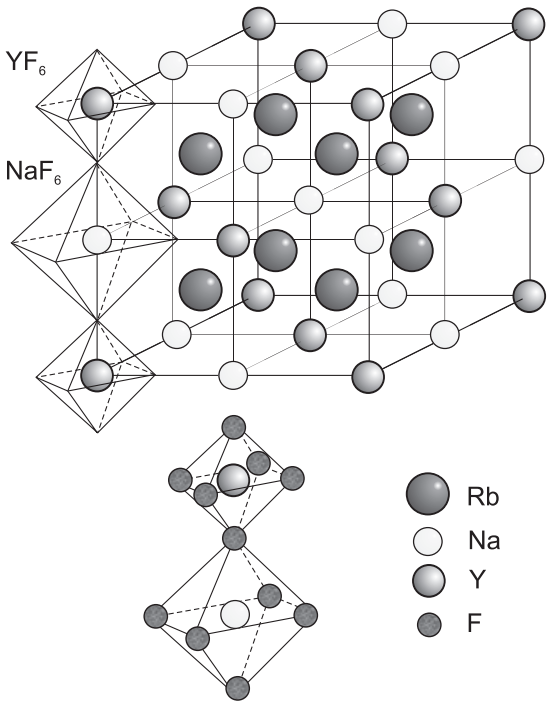

Figure 1. Cubic phase unit cell structure.

Table 1. Interatomic interaction potential parameters

Bond	λ, [aJ/Å]	ρ, [Å]
Rb–F	178.788	0.327037
Na–F	195.382	0.259152
Y–F	539.006	0.271506
F–F	−501.120	0.261946

High-pressure experiments (up to 4.33 GPa) were performed at 295 K in a diamond anvil cell[20] EasyLab LeverDAC Mini. A thoroughly dehydrated 1:4 methanol–ethanol mixture was used as a pressure-transmitting medium. The oriented crystal samples were placed in a chamber 250 μm in diameter and 100 μm thick. Pressure was monitored by the shift of the $^2F_g \rightarrow {}^4A_{2g}$ fluorescence band of Cr^{3+} ion in a small ruby crystal placed in the vicinity of the sample[21–23] within the experimental error of about 0.05 GPa. The birefringence effects were observed at the same time with a polarization microscope.

To analyze the low wavenumber Raman spectra quantitatively, we performed spectral analyses with a combination of conventional damped harmonic oscillator functions[24,25]:

$$I(\omega) = F(\omega, T) \cdot \sum_i \frac{2A_i \omega_{0i}^2 \gamma_i \omega}{\left(\omega_{0i}^2 - \omega^2\right)^2 + 4\gamma_i^2 \omega^2} \tag{1}$$

where ω_0, current wavenumber, A, ω and Γ denote the intensity, harmonic wavenumber of the band center and full width at half maximum (FWHM), respectively, of the corresponding excitation indicated by the subscript. The temperature factor $F(\omega,T)$ is calculated by

$$F(\omega, T) = \begin{cases} n(\omega) + 1 & \text{Stokes} \\ n(\omega) & \text{Anti} - \text{Stokes} \end{cases} \tag{2}$$

$$n(\omega) = \left[\exp\left(\frac{c\hbar\omega}{k_B T}\right) - 1\right]^{-1} \tag{3}$$

with the intensity interplay between the Stokes and anti-Stokes parts near 0 cm^{-1} is uniquely obtained according to the temperature. ħ, k_B and c in Eqn (3) are the reduced Planck constant, the Boltzmann constant and speed of light, respectively. The present Raman setup observes performed with dependence:

$$\Omega(T) = \omega_0 + A\left(1 + \frac{1}{\exp\left(c\hbar\Omega_{\beta 1}/k_B T\right) - 1} + \frac{1}{\exp\left(c\hbar\Omega_{\beta 2}/k_B T\right) - 1}\right) \tag{4}$$

which corresponds to decay into two phonons with wavenumbers $\Omega_{\beta 1}$ and $\Omega_{\beta 2}$ ($\omega_0 = \Omega_{\beta 1} + \Omega_{\beta 2}$).[26] Approximation of the lines damping constant has been performed with dependence:

Table 2. Wyckoff positions and irreducible representations (Γ-point phonon modes) for Rb_2NaYF_6 (space group $Fm\bar{3}m$, O_h^5, No. 225)

Atom	Wyckoff position	Γ-point phonon modes
Rb	8c	$F_{2g} + F_{1u}$
Na	4b	F_{1u}
Y	4a	F_{1u}
F	24c	$A_{1g} + E_g + F_{2u} + F_{2g} + 2F_{1u} + F_{1g}$

Modes classifications

$\Gamma_{\text{Raman}} = A_{1g} + E_g + 2F_{2g}$ $\quad$ $\Gamma_{\text{IR}} = 4F_{1u}$ $\quad$ $\Gamma_{\text{Acoustic}} = F_{1u}$ $\quad$ $\Gamma_{\text{Mehanical}} = A_{1g} + E_g + 2F_{2g} + 5F_{1u} + F_{2u} + F_{1g}$

Raman tensor

$$A_{1g} = \begin{bmatrix} a & 0 & 0 \\ 0 & a & 0 \\ 0 & 0 & a \end{bmatrix} \quad E_g = \begin{bmatrix} b & 0 & 0 \\ 0 & b & 0 \\ 0 & 0 & -2b \end{bmatrix} \quad E_g = \begin{bmatrix} -\sqrt{3}b & 0 & 0 \\ 0 & -\sqrt{3}b & 0 \\ 0 & 0 & 0 \end{bmatrix} \quad F_{2g} = \begin{bmatrix} 0 & 0 & 0 \\ 0 & 0 & d \\ 0 & d & 0 \end{bmatrix} \quad F_{2g} = \begin{bmatrix} 0 & 0 & d \\ 0 & 0 & 0 \\ d & 0 & 0 \end{bmatrix} \quad F_{2g} = \begin{bmatrix} 0 & d & 0 \\ d & 0 & 0 \\ 0 & 0 & 0 \end{bmatrix}$$

$$\Gamma(T) = \Gamma_0 + B\left(1 + \frac{1}{\exp(c\hbar\Omega_{\beta 1}/k_B T) - 1} + \frac{1}{\exp(c\hbar\Omega_{\beta 2}/k_B T) - 1}\right) \quad (5)$$

where ħ is reduced Planck constant, c is speed of light and k_B is the Boltzmann constant.

Calculation

To calculate Rb_2NaYF_6 vibrational spectrum, we used simulation package LADY (version of CRYME[27]). The best agreement between experimental values of atomic vibrations with the calculated values was obtained with the use of the 'hybrid model'.[28] This model is a combination of valence force field (VFF) and 'rigid-ion' models (RIM). We simulated complete spectra

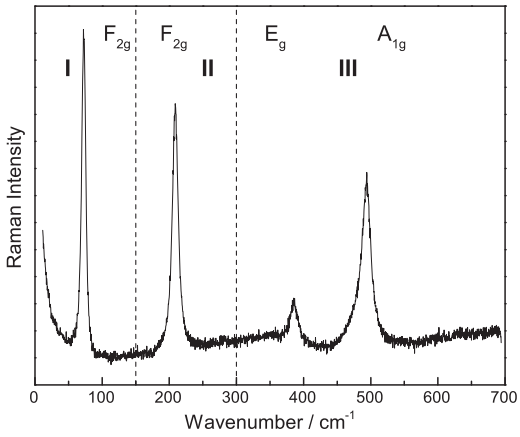

Figure 2. Cubic phase Raman spectrum (295 K).

Table 3. Assignments, band positions, approximation parameters, damping constants in cubic phase

Symm. type	Normal vibration modes CX_6 molecules [32]	Experim. Cs_2KYF_6[31] (cm^{-1})	Calcul. Rb_2NaYF_6 (cm^{-1})	Experim. Rb_2NaYF_6 295 K (cm^{-1})	ω_0, (cm^{-1})	A, (cm^{-1})	Γ_0, (cm^{-1})	B, (cm^{-1})	$\Omega_{\beta 1}$, (cm^{-1})	$\Omega_{\beta 2}$, (cm^{-1})
A_{1g}	ν_1 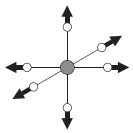	476	493	493	502.193	−0.850	5.521	1.169	251.096	251.097
E_g	ν_2 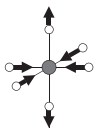	382	385	385	398.447	−0.879	2.736	0.791	128.378	270.069
F_{2g}	ν_5 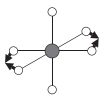	194	209	209	206.312	0.082	3.724	0.198	56.808	149.504
F_{2g}			72	73						
F_{1u}			0							
F_{1u}		80	86							
F_{1u}	ν_3 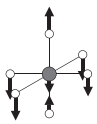	160	171							
F_{1u}	ν_4 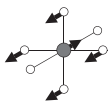	200	216							
F_{1u}			491							
F_{2u}	ν_6 		112							
F_{1g}			47							

of the crystals; interionic interactions between Rb–F, Na–F have been described in the fairly common model of 'rigid-ion', where interatomic potential is considered as a sum of long range Coulomb electrostatic:

$$V^{\mathrm{RIM}}(r_{ij}) = \frac{1}{2}\cdot\sum_{i,j}\frac{Z_iZ_j}{r_{ij}} + U(r_{ij}) \tag{6}$$

The short-range interaction potential was taken in the Born–Mayer form

$$U(r_{ij}) = \lambda\cdot\exp\left(-\frac{r_{ij}}{\rho}\right) \tag{7}$$

where r_{ij} is the interatomic distance, and λ and ρ are the parameters characterizing of the short-range pair interionic interaction. The values of λ and ρ are listed in Table 1. To obtain a satisfactory agreement of experimental and calculated results interactions within the octahedral groups CX_6 in crystals (interaction Y–F, F–F) potential function was composed as a sum of rigid-ion potential and the VFF potential. VFF model is applicable in describing the lattice dynamics of covalent, ionic and ionic-molecular crystals. Thus, for lattice dynamics calculations of crystals, the potential function takes the form

$$V(r_{ij}) = \frac{1}{2}\cdot\sum_{i,j}\frac{Z_iZ_j}{r_{ij}} + U(r_{ij}) + U_{\mathrm{VFF}} \tag{8}$$

Initial values of parameters were set at random within the ranges typical for the perovskite-like fluorides. Lattice stability conditions were taken into account. Resulting model parameters were obtained by minimization of residual values of the simulated and experimental Raman frequencies of the cubic phase using the Fletcher–Reeves method. In the case of suspension of the Fletcher–Reeves method because of the incompatible model parameters, initial parameters of the model were set randomly again.

Results and discussion

The vibration modes symmetry analysis[29,30] of the $Fm\bar{3}m$ structure of Rb_2NaYF_6 is presented in Table 2. Vibrational representation for the cubic phase at Brillouin zone center is

$$\begin{aligned}\Gamma_{\mathrm{vibr}} = {} & A_{1g}(xx,yy,zz) + E_g(xx,yy,zz) \\ & +2F_{2g}(xz,yz,xy) + F_{1g} + 5F_{1u} + F_{2u}\end{aligned} \tag{9}$$

where corresponding components of the Raman scattering tensor are given in brackets.

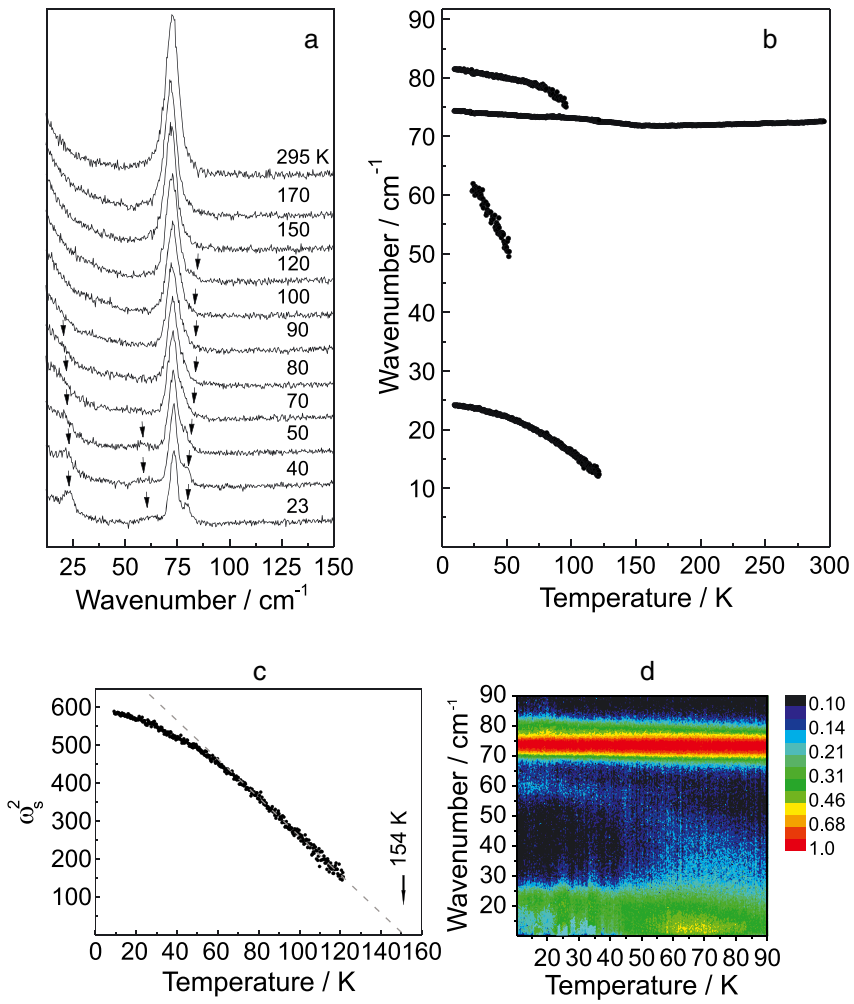

Figure 3. (a) Temperature transformation of low wavenumber modes. (b) Temperature dependences lattice modes positions. (c) Temperature dependence of squared soft mode wavenumber. (d) Raman intensity map in the low wavenumber region.

We have performed detailed investigation of Raman spectra of Rb_2NaYF_6 crystal under cooling from 300 to 8 K. Number of the lines observed in the cubic phase agrees well with predicted one by selection rules (Fig. 2). Full spectrum in cubic phase could be subdivided in three parts, corresponding to vibrations of structural elements:

I, region of lattice vibrations, $<150\,cm^{-1}$;

II, Y–F deformation region, 150–300 cm^{-1};

III, Y–F stretching region, 300–600 cm^{-1}.

Site symmetry of YF_6^{3-} ions coincides with the free ion symmetry. Symmetry and frequencies of the free ion vibrations are ν_1 (A_{1g}) – 476 cm^{-1}, ν_2 (E_g) – 382 cm^{-1}, ν_3 (F_{1u}) – 160 cm^{-1}, ν_4 (F_{1u}) – 200 cm^{-1}, ν_5 (F_{2g}) – 194 cm^{-1}, ν_6 (F_{2u}) – wavenumber unknown.[31,32] We might expect the splitting of the ν_2 (E_g) and ν_5 (F_{2g}) degenerate modes in the probable distorted phase and soft modes recovering below the transition from the cubic to this second phase. Lines at 493, 385 and 209 cm^{-1} (at 295 K) correspond to internal YF_6^{3-} modes: ν_1, ν_2 and ν_5, respectively. The wavenumber of the only Raman active lattice mode is 73 cm^{-1} at 295 K. Experimental vibrational modes of Rb_2NaYF_6 are given in Table 3 along with theoretical calculations. Totally symmetrical mode is underlined. Table 3 shows experimental band positions for Rb_2NaYF_6 and Cs_2KYF_6 cubic phase.[31] Natural positions of these bands for these crystals are slightly different.

Transformation of the lower wavenumber part of the spectrum is plotted in Fig. 3(a). The triply degenerated hard mode F_{2g}

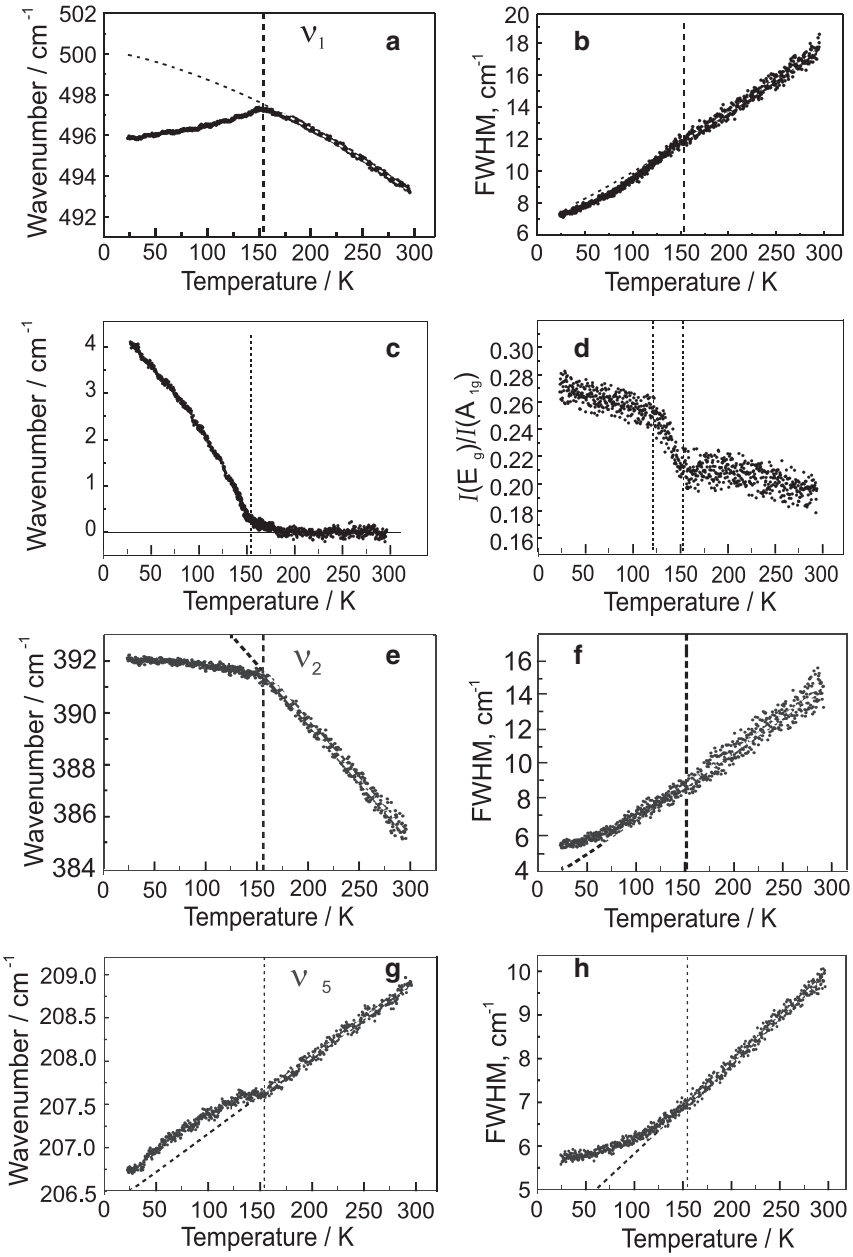

Figure 4. (a) Temperature dependence of the ν_1 internal mode positions. (b) Temperature dependence of the width (FWHM) ν_1 internal mode. (c) Wavenumber shift temperature dependence of the internal vibration with respect to the extrapolated value. (d) Relative intensity internal modes $I(E_g)/I(A_{1g})$ *versus* temperature. (e) Temperature dependence of ν_2 internal mode position. (f) Temperature dependence of the width (FWHM) ν_2 internal mode. (g) Temperature dependence of ν_5 internal modes positions. (h) Temperature dependence of the width (FWHM) ν_5 internal mode. Vertical dashed curves – phase transitions temperatures. Oblique dashed curves – data approximations in the cubic phase.

located in this region. Below 125 K appearance of weak three lines with maxima at 12, 50 and 76 cm^{-1} may be marked.

We fitted this part of the spectrum using damped harmonic oscillator functions (Eqns 1, 3, 4). Resulting temperature dependences of lines positions is shown in Fig. 3(b). Temperature transformation of two modes (12 and 50 cm^{-1}) may be considered as a soft mode behavior. Figure 3(c) describes the soft mode (at 12 cm^{-1}) reduced squared wavenumber[24] $\omega_s^2 \equiv \omega_{0s}^2 - \gamma_s^2$. The temperature dependence of squared soft mode wavenumber is extrapolated by linear function (dashed line on Fig. 3(c)) that is typical for soft modes at the second order phase transitions. Estimated temperature of this transition is about 154 K. The intensity of the second line at 50 cm^{-1} is very weak to perform such extrapolation for it. Figure 3(d) shows transformation of Raman intensity with temperature in this spectral region.

Besides lattice modes, we have studied spectra of YF $_6^{3-}$ group internal vibrations. Temperature dependence of ν_1 internal mode (A_{1g} symmetry) position and approximation of ν_1 (A_{1g}) internal mode positions with dependence, Eqn 4 is given in Fig. 4(a). Width of this line reveals some transitional effects as well. Its temperature dependence and approximation of the line 495 cm^{-1} damping constant with dependence, Eqn 5 is given in Fig. 4(b). The results of the approximations are presented in Table 3. Figure 4(c) shows temperature dependence of the shift of this internal mode with respect to the extrapolated value $\Delta\omega(T)$. For non-degenerate hard modes $\Delta\omega(T) \sim \eta^2$ (T), where η denotes order parameter.[33,34] A small additional shift of the line position appears even in the cubic phase in a rather narrow (about 20 K) region above the phase transition point $T_1 = 154$ K. The shift increases steadily in the cubic phase under cooling and becomes linear in the second phase that corresponds to a second-order phase transformation. The experimental dependence is seen to be correctly described by this expression. This fact indicates the absence of substantial structural disordering contributions in the high temperature phase.

The line corresponding to ν_2 (E_g) internal mode is the weakest one in the spectrum of the cubic phase (Fig. 2). Temperature dependences of its position and width are shown in Fig. 4(e,f). The line position increases from 385 to 391 cm^{-1} with cooling in cubic phase. After the transition point (154 K), line position goes up slowly with cooling. Approximation of ν_2 mode position, Eqn 4 is shown by dashed line in Fig. 4(e). Line width continuously decreases with cooling as shown in Fig. 4(f). Approximation of the line damping constant, Eqn 5 is shown by dashed line in Fig. 4(f). The fitted dependence corresponds to the phonon decay into two optical phonons (Table 3).

Temperature dependences of the line position and the width in the region of F_{2g} mode are given in Fig. 4(g, h). Position of the line changes from 209 to 207.5 cm^{-1} under cooling to 154 K and remains practically constant (207.5 cm^{-1}) within 154 to 146 K. Below 146 K, the line position drops slightly to 206.7 cm^{-1}. Line width decreases continuously under cooling within the whole studied temperature region. The temperature dependence of F_{2g} mode position approximated with the Eqn 4 in cubic phase is shown in Fig. 4(g) (dashed curves). The temperature dependence of F_{2g} line width approximation by the Eqn 5 in cubic phase is shown in Fig. 4(h) (dashed curves). The parameters of the approximation of this mode positions in cubic phase are presented in Table 3.

Close positions of ν_1 and ν_2 lines provide a possibility to measure their relative intensity. The result is shown in Fig. 4(d). This ratio grows continuously under cooling, but its temperature dependence shows two noticeable anomalies, at 154 and 122 K. This second anomaly may be attributed to one more phase transition at this temperature.

The transformation of the polarized Raman spectra under hydrostatic pressure is shown in Fig. 5. Slight polarization violation is observed under pressure because of the stresses in the diamond anvils (Fig. 5a, b). The dependencies line positions *versus* pressure are plotted in Fig. 6. They move up evenly. The peak 385 cm^{-1} is very weak. We could not define its positions at pressure upper 3.2 GPa correctly. The wavenumber

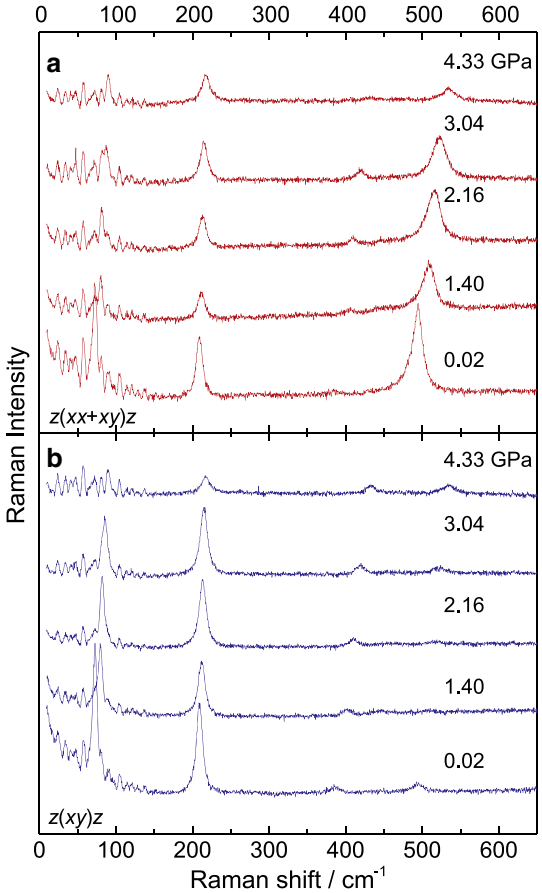

Figure 5. Pressure induced transformations Raman spectra.

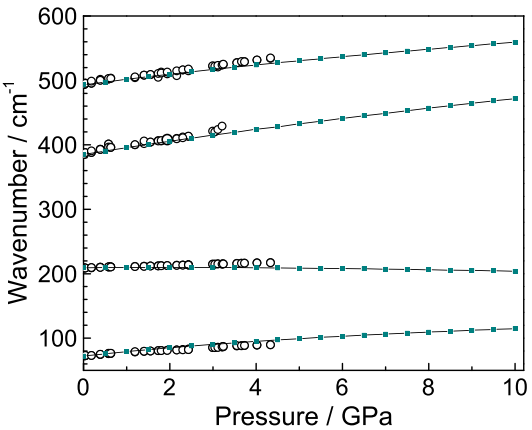

Figure 6. Experimental (circles) and calculated (squares) lines positions *versus* the pressure.